Check for updates

Quantum metasurfaces with atom arrays

R. Bekenstein [1,2 ✉], I. Pikovski[1,2,3,4], H. Pichler[1,2], E. Shahmoon[2,6], S. F. Yelin[2,5] and M. D. Lukin [2]

Metasurfaces mould the flow of classical light waves by engineering subwavelength patterns from dielectric or metallic thin films. We introduce and analyse a method in which quantum operator-valued reflectivity can be used to control both the spatiotemporal and quantum properties of transmitted and reflected light. Such quantum metasurfaces are realized by entangling the macroscopic response of atomically thin atom arrays to light. We show that such a system allows for parallel quantum operations between atoms and photons as well as for the generation of highly entangled photonic states such as photonic Greenberger–Horne–Zeilinger and three-dimensional cluster states suitable for quantum information processing. We analyse the influence of imperfections as well as specific implementations based on atom arrays excited into Rydberg states.

In the past decade, significant effort has been directed towards structuring classical light waves using spatial light modulators and metasurfaces[1–9]. Such structured light has many potential applications, ranging from micromachining to manipulating particles[10–12]. Furthermore, it can affect interactions in nonlinear optical systems[13]. Recently, an implementation of metasurfaces using arrays of atoms has been studied[14–18], and metasurfaces have been employed to manipulate photonic quantum states[19,20]. Moreover, a new approach for entangling atom arrays has been suggested[21]. Although previous efforts have focused on structuring the spatial or temporal properties of light by means of metasurfaces[22], here we explore the possibility for generating atom–photon entanglement between metasurfaces and photons and using it for controlling the many-body entangled photonic state. Such 'quantum metasurfaces' are realized by preparing and manipulating entangled states of atomic reflectors and scattering light from them, constituting a new platform for manipulating both classical and quantum properties of light.

Here we analyse, in particular, a method in which quantum operator-valued reflectivity allows us to simultaneously control the quantum and spatiotemporal properties of light in free space. This approach can be used to realize a quantum light modulator (QLM), enabling the generation of highly correlated photonic states. As example applications, we show that this methodology enables cavity-free parallel quantum operations on multiple photonic degrees of freedom and the preparation of highly entangled photonic states suitable for quantum information, such as multidimensional photonic cluster states.

Quantum metasurfaces. The key idea of this work is to manipulate the macroscopic response of a metasurface to light on a quantum level. This results in atom–photon entanglement and allows for quantum light state manipulation. Specifically, we focus on the realization of such quantum metasurfaces using two-dimensional (2D) arrays of neutral atoms. Such an approach has the advantage that even a single atomic layer can have extreme scattering properties, where using subwavelength spacing of atoms results in perfect reflectivity for some frequencies of light[14,15]. At the same time, the internal atomic degrees of freedom and, correspondingly, the scattering properties of such an array, can be easily manipulated.

In combination, these two properties allow us to manipulate the quantum properties of light in a free-space setting. To illustrate this, let us assume that we can prepare the atom array in two quantum states: a state $|C\rangle$, in which the array is coupled to an incident light field, and a second state $|U\rangle$, in which it is uncoupled and thus transparent. Specific implementations to achieve such control are discussed in the following. Scattering a coherent light beam off a quantum metasurface prepared in a superposition state $|\psi\rangle = \frac{1}{\sqrt{2}}(|U\rangle + |C\rangle)$ results in entanglement between the quantum metasurface and the free-space photonic degrees of freedom:

$$|\Psi\rangle = |U\rangle \otimes |\alpha, 0\rangle + |C\rangle \otimes |t\alpha, r\alpha\rangle) \tag{1}$$

where r and t are the reflection and transmission coefficients identified with the linear response of the atom array. Further control can be obtained by measuring the state of the array (Fig. 1a,c). For example, a projective measurement in the basis of entangled states $\frac{1}{\sqrt{2}}(|U\rangle \pm |C\rangle)$ projects the conditionally scattered light into cat-like states: $|\psi\rangle = \frac{1}{\sqrt{2}}(|\alpha, 0\rangle \pm |t\alpha, r\alpha\rangle)$.

To achieve quantum control over the scattering properties of an atom array, we consider atoms with three internal levels, a ground state $|g\rangle$, an excited state $|e\rangle$ and a Rydberg state $|r\rangle$ (Fig. 1b). We are interested in the situation where state $|g\rangle$ is coupled by an optical dipole transition to state $|e\rangle$. Using an appropriate (subwavelength) arrangement of atoms, the array acts as a mirror for photons tuned to the collective resonance around the $g \leftrightarrow e$ transition frequency, ω_{eg}, realizing the coupled state ($|C\rangle$) (Fig. 1c). The array can be turned transparent by means of electromagnetically induced transparency (EIT) by applying a classical coherent pump field with frequency ω_p that coherently couples the state $|e\rangle$ to the state $|r\rangle$, with Rabi frequency Ω_p. The switch between reflective and transparent response of the array consists of an ancillary atom and employs Rydberg interactions to control the two-photon resonance frequency (similar to the so-called 'Rydberg blockade' mechanism[23]). The ancillary atom has two internal states, a ground state $|g'\rangle$ and a Rydberg state $|r'\rangle$. We assume that it can be trapped in close proximity to the atom array, such that it interacts strongly with any atom in the array, if both are in the Rydberg states $|r'\rangle$ and $|r\rangle$, respectively[24,25]. We denote the corresponding interaction shift by V.

[1]ITAMP, Harvard-Smithsonian Center for Astrophysics, Cambridge, MA, USA. [2]Physics Department, Harvard University, Cambridge, MA, USA. [3]Department of Physics, Stevens Institute of Technology, Hoboken, NJ, USA. [4]The Oskar Klein Centre, Department of Physics, Stockholm University, Stockholm, Sweden. [5]Department of Physics, University of Connecticut, Storrs, CT, USA. [6]Present address: Department of Chemical & Biological Physics, Weizmann Institute of Science, Rehovot, Israel. ✉e-mail: rivka.bekenstein@cfa.harvard.edu
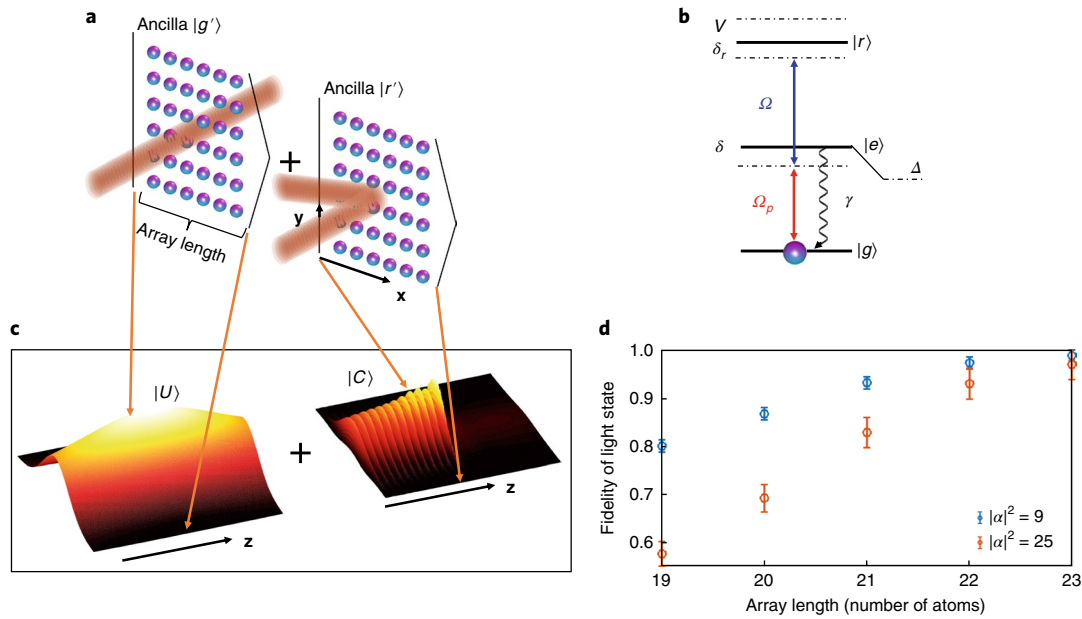
Fig. 1 | Preparing cat states with quantum metasurfaces. a, Schematic of scattering from the quantum metasurface in a superposition state that perfectly reflects (coupled) and perfectly transmits (uncoupled) the light tuned close to the collective $|g\rangle \rightarrow |e\rangle$ transition (with collective shift Δ), conditioned on the ancilla state. **b,** Electronic levels for EIT implementation of a two-photon cascade configuration where a control field tuned to the $|e\rangle \rightarrow |r\rangle$ transition is applied, resulting in an array transparent to light tuned to the collective $|g\rangle \rightarrow |e\rangle$ transition. If $|r\rangle$ is shifted due to the interaction with an ancilla, the EIT condition is not fulfilled and the quantum metasurface is reflective. **c,** Numerical calculation of the electric field distribution after scattering from the quantum metasurface in the coupled (right) and uncoupled (left) state. **d,** Effect of a finite array: the fidelity of the cat light state, calculated after projective measurement of the quantum metasurface state (see Supplementary Information), as a function of atom array length (for a spacing of 0.2λ and Gaussian beam waist of 1.56λ). Error bars represent errors in the extraction of reflection and transmission coefficients from numerical calculations (see Supplementary Information for more details).

The ancillary atom acts as a quantum switch, controlling the reflection coefficient of the atom array:

$$r = \frac{i(\gamma + \Gamma)(\delta_r + V)}{-i(\delta_r + V)(\gamma + \Gamma - 2i(\delta - \Delta)) + 2|\Omega_p|^2} \quad (2)$$

where $\delta = \omega_{eg} - \omega$ is the detuning of the light from the atomic resonance and γ denotes the radiative lifetime of state $|e\rangle$. Δ and Γ are cooperative corrections to δ and γ, arising from dipole–dipole interactions, and $\delta_r = \omega_{rg} - \omega_p - \omega$ is the two-photon detuning (see Supplementary Information for details). We are interested in the scattering properties of incident photons that are resonant with the cooperatively renormalized transition frequency, that is $\delta = \Delta$. If the ancillary atom is in the ground state, the array is completely transparent, with $r = 0$, realizing $|U\rangle$ (for pump frequency satisfying $\delta_r = 0$). On the other hand, if the ancillary atom is in the Rydberg state, the two-photon resonance is effectively shifted by V such that the array becomes reflective:

$$r \rightarrow -1 + i\frac{|\Omega_p|^2}{(\gamma + \Gamma)/2}\frac{1}{V} \quad (3)$$

realizing $|C\rangle$. Thus, far away from the two-photon resonance $r \xrightarrow{V \rightarrow \infty} -\frac{(\gamma + \Gamma)/2}{(\gamma + \Gamma)/2 - i(\delta - \Delta)}$, the reflection coefficient reduces to $r = -1$ at $\delta = \Delta$. We emphasize that cooperative effects arising from diople–dipole interactions within the array play a fundamental role in the scattering dynamics. Furthermore, note that at this stage we neglect any spatial dependence of the Rydberg interaction V across the array, where the above results holds as long as $V \gg \frac{|\Omega_p|^2}{(\gamma + \Gamma)/2}$.

Using this approach, the superposition is realized by preparing the ancillary atom in the superposition $\frac{1}{\sqrt{2}}(|g'\rangle + |r'\rangle)$. Further

control can be obtained by 'measurements' of the array state, which in this context corresponds to ancilla measurement in the appropriate basis: $\frac{1}{\sqrt{2}}(|g'\rangle \pm |r'\rangle)$. Although perfect reflectivity is valid in the case of infinite arrays, in practice, control over atom arrays of modest size is sufficient to produce relatively large cat-like states with high fidelity (Fig. 1d).

Applications to photonic quantum state control. This quantum metasurface provides a light–matter interface that allows high-fidelity control over quantum light states by generalizing protocols discussed in the context of cavity quantum electrodynamics (QED)[26–29] to a free-space setting (Fig. 2a), while removing major loss channels that limit cavity-based approaches and also allowing for natural parallelization as multiple transverse modes of the light can be controlled simultaneously. As a specific example, we consider several non-overlapping Gaussian beams, focused onto different transverse locations (n, m) of the quantum metasurface. Here, single photons in each of the transmitted and reflected modes represent qubit states $|0\rangle_{n,m}$ and $|1\rangle_{n,m}$, respectively. An ancillary atom that controls the reflectivity of the entire array allows one to simultaneously manipulate these qubits and realize multi-qubit gates. Specifically, this allows one to entangle photons in different transverse locations in a single scattering process, as shown in Fig. 2a. With the control qubit in state $\frac{1}{\sqrt{2}}(|g'\rangle + |r'\rangle)$, the scattering of N_{ph} incident unentangled photons, followed by a projective measurement of the ancillary atom in the basis $\frac{1}{\sqrt{2}}(|g'\rangle \pm |r'\rangle)$, prepares an N-photon entangled Greenberger–Horne–Zeilinger (GHZ) photonic state $|\psi_{GHZ}\rangle = \frac{1}{\sqrt{2}}(|0\rangle^{\otimes N_{ph}} + |1\rangle^{\otimes N_{ph}})$. In this configuration, the scattering process realizes a parallel controlled-NOT (CNOT) gate for many photonic qubits (Fig. 2c). The extent to which such operations can be parallelized is mainly limited by the finite range for
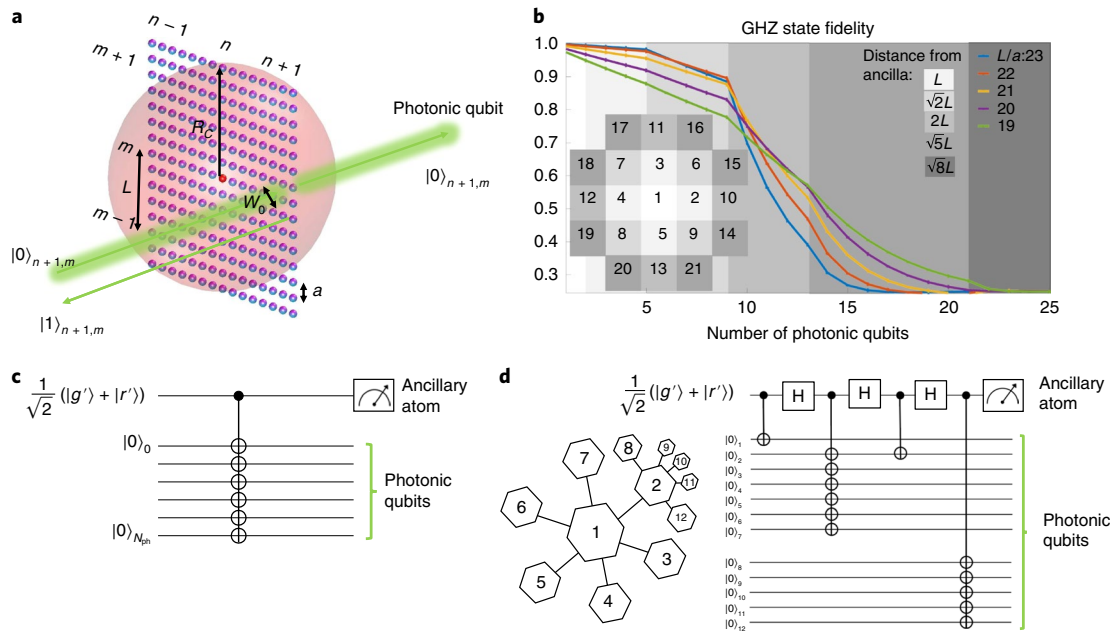
Fig. 2 | Quantum information with quantum metasurfaces. a, A central ancillary atom (red) controls multiple photonic qubits by scattering from a quantum metasurface. Photonic qubits are defined as right ($|0\rangle_{n,m}$) or left ($|1\rangle_{n,m}$) propagating modes in transverse locations (n,m). **b**, Lines: fidelity of the photonic GHZ state as a function of photonic qubit number for different mode separation distances (L/a) (where a is the atomic spacing). The fidelity is affected by the strength of the interaction with the central ancilla and the collective reflectivity. For larger mode separation (blue), the fidelity drops faster with photonic qubit number due to the finite Rydberg interaction. Inset: schematic of the photons' transverse location (bottom left), where the greyscale reflects the distance from the central ancilla, which corresponds to coloured areas in the fidelity graph, each with a specific slope. The fidelity is evaluated for interaction strength $R_c/a = 57$ and mode width $W_0 = 1.56\lambda$ (see Supplementary Information for more examples). **c,d**, Quantum circuits of preparation protocols for the photonic entangled states described in the main text (for the GHZ state (**c**) and the tree cluster state (**d**)), where qubit numbering is in agreement with the graph representation in **b**.

which the Rydberg interactions efficiency control the EIT condition of the transverse modes (Fig. 2b). To maximize the spatial extend of the Rydberg blockade it may be beneficial to use Rydberg states of different parity, such as P and S states for ancillary and array atoms, respectively[24,25].

As the quantum metasurface enables parallelization of quantum operations on multiple qubits, it offers a natural platform for fast preparation of tree cluster states, which are tensor network states with preparation protocols consisting of parallel control gates (Fig. 2d). These types of entangled state are important for overcoming photon loss errors[30] and as part of quantum error correction schemes, and they can serve as a basic building block to states related to holographic high-energy theories[31]. In particular, Fig. 2d displays the graph representation of a state where each single qubit is connected to six others. The protocol consists of initializing the ancillary atom in the $\frac{1}{\sqrt{2}}(|g'\rangle + |r'\rangle)$ state. In each step, photons in specific transverse locations are scattered from the array to create the desired correlations, where in between steps the state of the ancilla is rotated (Hadamard gate), marked by boxed H). This procedure consists of rescattering specific photons from the quantum metasurface, which can be implemented by employing free-space techniques (see Supplementary Information). The quantum metasurface can also serve as a building block for a scalable quantum optical interface. This can be implemented by considering an array of quantum metasurfaces that act as photonic sources, as analysed in the next section.

Highly entangled photonic states via a QLM. The set-up described above can not only be used as a passive device but also as a source of quantum light in free space. In this mode of operation, the atom array effectively serves as an antenna[32] that emits single photons in

well-defined spatial modes. This emission process can be controlled by the ancillary atom, enabling the generation of quantum correlations between sequentially generated photons. This system can be scaled to generate large-scale atom–photon entanglement. In particular, one can envision its use as a QLM with multiple ancillary atoms, each controlling its own array (pixel), which serves as the interface to free-space photons (as schematically depicted in Fig. 3c). The specific protocol for controlled quantum emission from a single pixel consists of two steps. First, a coherent pulse (with Rabi frequency Ω_1) is used to resonantly excite the atoms in the array to a single delocalized Rydberg excitation (Fig. 3a)[23], conditioned on the ancillary atom state. Next, a control field (Ω_2) is applied to transfer the Rydberg excitation to the collective excited state. The radiative decay of this collective excitation results in photon emission with defined momentum[33] due to momentum conservation of the collective excitation (see Supplementary Information for details). In summary, the conditional emission of a photon results in the ancilla-photon entangled state $\alpha|g'\rangle + \beta|r'\rangle \rightarrow \alpha|g',1\rangle + \beta|r',0\rangle$, where $|0\rangle$ and $|1\rangle$ refer to the presence or absence of a photon. The fidelity for the controlled emission is displayed in Fig. 3b as a function of pixel size and for typical Rydberg blockade. This approach allows for the preparation of desired entangled states of the ancillary atoms that control the emission from the different pixels of the QLM, enabling generation of photonic correlations between many degrees of freedom. In this setting, the quantum information is encoded in the absence or presence of photons in specific transverse locations. In addition, by sequential operations we can employ photon state engineering schemes in the time degree of freedom[34–36].

As a specific example, we describe the preparation protocol for a 3D photonic cluster state, which has important applications for fault-tolerant quantum computation[37]. The first step is to prepare a

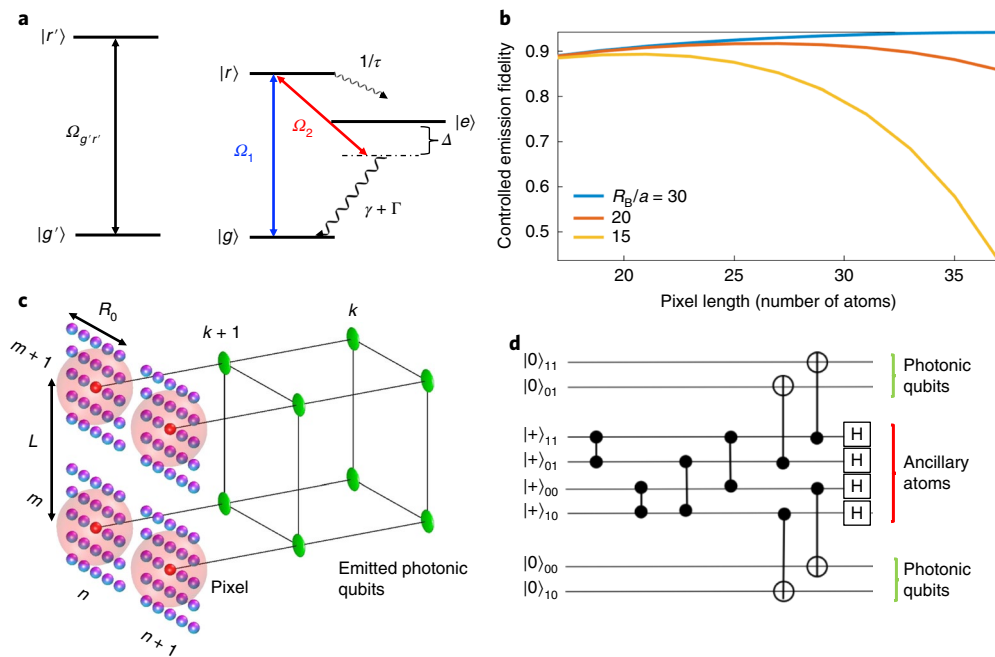**Fig. 3 | QLM for highly entangled free-space photons. a**, A single array (pixel) as a conditional single-photon source, showing electronic levels of the corresponding control ancilla (left) and a typical atom within the array (right). Two control fields Ω_1, Ω_2 are applied for generating photon emission from the collective excited state through the Rydberg state, which is conditioned on the ancilla state due to Rydberg blockade. **b**, Fidelity of the emitted photon state as a function of pixel size, for different Rydberg blockade radii (R_B). The fidelity is limited by the finite blockade radius and emission to undesired modes (finite Rydberg lifetimes are neglected, assuming fast procedures). **c**, Schematic of 2×2 pixels of the QLM, where each pixel emits a photon (green) controlled by the corresponding ancillary atoms (red), which Rydberg blockades the pixel (light red) conditioned on its state. The many-body ancilla state controls the correlation of the emitted photons. **d**, An example of 3D photonic cluster state preparation. The quantum circuit describes the protocol for emission of 2D cluster states for $N = 2$, $M = 2$. K times repetition of this protocol generates a 3D cluster state of $N \times M \times K$ photonic qubits.

2D atomic cluster state for the array of ancillary atoms. This is done by initializing the ancillary atoms in the $|+\rangle = (|g'\rangle + |r'\rangle)/\sqrt{2}$ state and applying entangling gates (controlled phase gates) between neighbouring ancillary atoms, for example by exciting them to Rydberg states[38] (Fig. 3d). By applying the protocol for controlled emission described above, single photons are emitted from each pixel, conditioned on the state of the corresponding ancilla. To sequentially generate photons, the ancillary atoms have to be re-entangled by rotation and repetition of the controlled phase gates from the first step. By repeating this protocol, the photonic cluster state dimension is increased (Fig. 3c), where with each repetition an additional $N \times M$ photons are entangled. Measuring the atomic state projects the system onto a photonic cluster state with an additional dimension (emission time) over the initial atomic cluster state dimension[39]. An illustration of the multi-qubit operation and the quantum circuit describing the 3D cluster state preparation is provided in Fig. 3c,d.

Potential implementations. We now discuss a specific realization of a quantum metasurface with an array of trapped neutral atoms[40–42] whose many-body state can be manipulated by exploiting Rydberg interactions[43,44]. Recently, the generation of superposition states of a 1D atom array was demonstrated[45]. An extension of this approach to two dimensions is sufficient for implementing the ancillary atoms controlling the QLM pixels. To realize the collective effect of the quantum metasurface, atoms have to be trapped at distances (a) that are smaller than the wavelength of the incident light ($\lambda > a$). For atom trapping with optical tweezers, the spacing between atoms is normally bounded by the diffraction limit. However, the requirement for subwavelength spacing can be met by

using longer-wavelength transitions where $\lambda > 1\,\mu m$ (for example, ^{171}Yb, which has a telecom transition of 1,389 nm, was recently trapped in optical tweezers using a 470 nm laser; ref. [46]). This enables the following realization of the electronic levels: $|g\rangle \equiv 6s6p^3P_0$ and $|e\rangle \equiv 5d6s^3D_1$. Recently, atomic confinement in optical lattices[47] has been utilized to demonstrate reflectivity from atomic arrays. Finally, we note that the condition for the subwavelength atom spacing can be relaxed if each pixel of the QLM is associated with a small atomic ensemble that can be used, under conditions of Rydberg blockade, to emit single photons with defined momentum[33,48].

Decoherence and fidelity analysis. We identify several main sources for decoherence and errors in our suggested system. First, the suggested protocols rely on Rydberg interactions, which have a finite range, inducing decoherence. These include the control mechanism of the ancillary atom, which is based on the Rydberg level shift of atoms within the array, and the single-photon source protocol, which relies on a maximum of one Rydberg excitation within the array. From a different perspective, the long-range Rydberg interactions can also induce decoherence due to crosstalk between foreign qubits. Another decoherence mechanism is the emission or scattering to undesired modes, which occurs for finite array sizes or for imperfect atomic states due to experimental limitations. For example, imperfect arrays result from unsuccessful atom trapping or atomic motion due to thermal fluctuations. In addition to these consideration, the finite lifetime of excitations to the Rydberg state also induces decoherence.

We estimate errors in state preparation quantitatively as follows. First, the inhomogeneous shift from resonance of the Rydberg level for atoms within the array results in imperfect reflectivity.
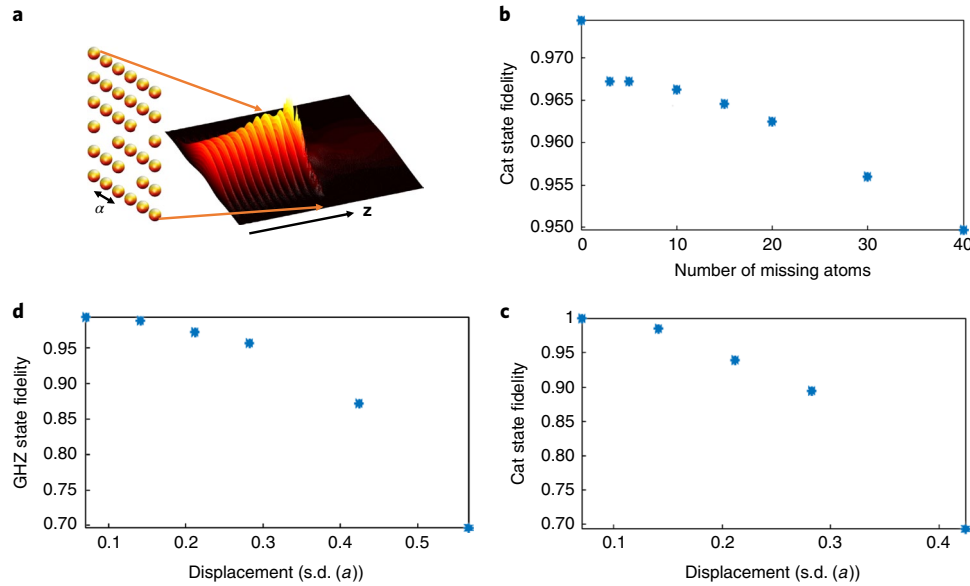
Fig. 4 | Error estimation from an experimental considerations. a, Left: schematic of an array with an example error of missing atoms. Right: calculated electric field distribution for scattering from a quantum metasurface with 10% missing atoms. **b**, Fidelity of the final cat light state after measuring the atom array state for an array of 23^2 atoms ($|\alpha|^2 = 9$) as a function of the number of missing atoms. The displayed results are averaged over the required number of random realizations of missing atoms, for convergence. **c,d**, Fidelity of the cat state ($|\alpha|^2 = 9$) (**c**) and the three-photon GHZ state calculated for an array of 23^2 atoms as a function of the s.d. of atom displacement due to thermal fluctuations.

For the cat state protocol we estimate the error probability $P \approx \frac{1}{8}\left|\frac{\Omega_p^2}{(\gamma+\Gamma)/2}\left(\frac{R^6}{c_6}\right)\right|^2|\alpha|^2$, where R is the average distance of atoms from the ancilla and c_6 is a constant that depend on the specific Rydberg level. For controlled reflection for photonic modes at distances r_{nm} from the ancilla, the error in the reflection coefficient is $\sim \frac{1}{-i(R_c/r_{nm})^6+1}$, where $R_c = \left(\frac{c_6(\gamma+\Gamma)}{2|\Omega_p|^2}\right)^{1/6}$. The finite Rydberg interactions also give rise to a non-vanishing probability for more than one Rydberg excitation within the array, resulting in decoherence for the emission protocol, estimated by $P \approx \sum_{i,j}\Omega_1|\mathbf{r}_i - \mathbf{r}_j|^6/N_a(N_a - 1)c_6$, where the sum runs over all atomic couples in the array and N_a is the total number of atoms. To estimate the error due to finite array sizes, we evaluate the imperfect reflectivity numerically by solving the scattering problem and quantify it by η_s (where $\eta_s = 1$ for perfect reflectivity), which depend on the mode width W_0 and the separation between modes L (see Supplementary Information and Fig. 2b). We estimate the emission to undesired non-paraxial modes by small array sizes (R_0) as $-\epsilon\lambda/R_0$, where $\epsilon = \pi - 1/\pi$ and λ is the photon wavelength. The finite lifetime of the Rydberg state induces decoherence, which is estimated by $-\left(\frac{1}{\Omega_1} + \frac{1}{\Omega_2}\right)/\tau_{g'r'}$ for the lifetime of the control ancilla ($\tau_{g'r'}$) and $-\frac{1}{\Omega_2\tau}$ for the lifetime of a collective excitation in the array (τ). We further consider the crosstalk between different qubits for the different protocols. For parallel quantum operations by one control atom, we estimate the crosstalk of the n,m qubit with foreign photonic modes by the overlap of the transverse wavefunctions $\int\int f_{nm}(x,y)\sum_{i,j\neq n,m}f^*_{ij}(x,y)dxdy$, where f_{ij} is the photonic wavefunction in transverse location ij, and $dxdy$ runs over the array area. For Gaussian wavefunctions this gives an error probability of $P \approx 0.0035$ per photonic qubit for $L = 1.8W_0$. For the QLM, we estimate the crosstalk by the effect of a Rydberg excitation in one array on the controlled emission from a foreign array. This gives a geometrical limit on the construction of the QLM, $L \gg \sqrt{2}R_0$, meaning that the distance between pixels has to be much larger than the pixel size. The above considerations are incorporated into the fidelity calculations that are displayed in Figs. 1d, 2b, 3b and 4 for the photonic cat state, GHZ state and controlled emission, respectively. For typical parameters, the fidelity of

the operation displayed in Fig. 2d is $F \approx 0.94$ for $L/W_0 = 23$. The fidelity of the 3D cluster state generation described above scales with photonic qubits number, $\mathcal{F}_{cs} = (\mathcal{F}_e)^{NMK}$, where $\mathcal{F}_e$ is the controlled emission fidelity shown in Fig. 3b, $N \times M$ is the number of ancillary atoms and K is the repetition number. Fidelity from imperfect preparation of atomic states is displayed in Fig. 4. For less than 1% of missing atoms, which is a typical error in the experimental systems[43,49], the cat state fidelity is still higher than 0.965. For displacement fluctuations that are smaller than $0.3a$, the three-photon GHZ state fidelity is higher than 0.96. The displacement fluctuation error can be further reduced by preparing the atoms in the motional ground state of an optical lattice potential[50], or utilizing a small atomic ensemble for each QLM pixel[23].

Outlook. The above considerations indicate that quantum metasurfaces can be used as an effective tool to create photonic quantum states. These considerations can be extended by combining techniques of classical metasurfaces for controlling the light degrees of freedom, such as angular momentum or polarization[51]. In particular, the QLM combines the parallelism of classical metasurfaces, as employed for applications such as equation solving[52] with quantum state control. Our analysis can be further extended to interactions between photons beyond the weak field limit[53,54]. We also note that other possible experimental realizations, including excitons in atomically thin semiconductors, such as transition metal dichalcogenides[55,56], can also be explored to realize quantum metasurfaces. Finally, we note that these considerations could be extended to quantum metamaterials and to explore phenomena such as emulations of the quantum gravitational background for light (see Supplementary Information).

Online content
Any methods, additional references, Nature Research reporting summaries, source data, extended data, supplementary information, acknowledgements, peer review information; details of author contributions and competing interests; and statements of data and code availability are available at https://doi.org/10.1038/s41567-020-0845-5.

References

1. Bomzon, Z., Biener, G., Kleiner, V. & Hasman, E. Space-variant Pancharatnam–Berry phase optical elements with computer-generated subwavelength gratings. *Opt. Lett.* **27**, 1141–1143 (2002).
2. Yu, N. et al. Light propagation with phase discontinuities: generalized laws of reflection and refraction. *Science* **334**, 333–337 (2011).
3. Kildishev, A. V., Boltasseva, A. & Shalaev, V. M. Planar photonics with metasurfaces. *Science* **339**, 1232009 (2013).
4. Chen, H.-T., Taylor, A. J. & Yu, N. A review of metasurfaces: physics and applications. *Rep. Prog. Phys.* **79**, 076401 (2016).
5. Rubinsztein-Dunlop, H. et al. Roadmap on structured light. *J. Opt.* **19**, 013001 (2016).
6. Kuznetsov, A. I., Miroshnichenko, A. E., Brongersma, M. L., Kivshar, Y. S. & Luk'yanchuk, B. Optically resonant dielectric nanostructures. *Science* **354**, aag2472 (2016).
7. Li, G., Zhang, S. & Zentgraf, T. Nonlinear photonic metasurfaces. *Nat. Rev. Mater.* **2**, 17010 (2017).
8. Khorasaninejad, M. & Capasso, F. Metalenses: versatile multifunctional photonic components. *Science* **358**, eaam8100 (2017).
9. Krasnok, A., Tymchenko, M. & Alu, A. Nonlinear metasurfaces: a paradigm shift in nonlinear optics. *Mater. Today* **21**, 8–21 (2018).
10. Yao, A. M. & Padgett, M. J. Orbital angular momentum: origins, behavior and applications. *Adv. Opt. Photon.* **3**, 161–204 (2011).
11. Mathis, A. et al. Micromachining along a curve: femtosecond laser micromachining of curved profiles in diamond and silicon using accelerating beams. *Appl. Phys. Lett.* **101**, 071110 (2012).
12. Schley, R. et al. Loss-proof self-accelerating beams and their use in non-paraxial manipulation of particles' trajectories. *Nat. Commun.* **5**, 5189 (2014).
13. Bekenstein, R., Schley, R., Mutzafi, M., Rotschild, C. & Segev, M. Optical simulations of gravitational effects in the Newton–Schrödinger system. *Nat. Phys.* **11**, 872–878 (2015).
14. Bettles, R. J., Gardiner, S. A. & Adams, C. S. Enhanced optical cross section via collective coupling of atomic dipoles in a 2D array. *Phys. Rev. Lett.* **116**, 103602 (2016).
15. Shahmoon, E., Wild, D. S., Lukin, M. D. & Yelin, S. F. Cooperative resonances in light scattering from two-dimensional atomic arrays. *Phys. Rev. Lett.* **118**, 113601 (2017).
16. Zhou, M., Liu, J., Kats, M. A. & Yu, Z. Optical metasurface based on the resonant scattering in electronic transitions. *ACS Photonics* **4**, 1279–1285 (2017).
17. Facchinetti, G. & Ruostekoski, J. Interaction of light with planar lattices of atoms: reflection, transmission and cooperative magnetometry. *Phys. Rev. A* **97**, 023833 (2018).
18. Wang, B., Zhao, C., Kan, Y. & Huang, T. Design of metasurface polarizers based on two-dimensional cold atomic arrays. *Opt. Exp.* **25**, 18760–18773 (2017).
19. Wang, K. et al. Quantum metasurface for multiphoton interference and state reconstruction. *Science* **361**, 1104–1108 (2018).
20. Stav, T. et al. Quantum entanglement of the spin and orbital angular momentum of photons using metamaterials. *Science* **361**, 1101–1104 (2018).
21. Guimond, P.-O., Grankin, A., Vasilyev, D. V., Vermersch, B. & Zoller, P. Subradiant Bell states in distant atomic arrays. *Phys. Rev. Lett.* **122**, 093601 (2019).
22. Weiner, A. M. Femtosecond pulse shaping using spatial light modulators. *Rev. Sci. Instrum.* **71**, 1929–1960 (2000).
23. Saffman, M., Walker, T. G. & Mølmer, K. Quantum information with Rydberg atoms. *Rev. Mod. Phys.* **82**, 2313 (2010).
24. Barredo, D. et al. Demonstration of a strong Rydberg blockade in three-atom systems with anisotropic interactions. *Phys. Rev. Lett.* **112**, 183002 (2014).
25. Browaeys, A., Barredo, D. & Lahaye, T. Experimental investigations of dipole–dipole interactions between a few Rydberg atoms. *J. Phys. B* **49**, 152001 (2016).
26. Knill, E., Laflamme, R. & Milburn, G. J. A scheme for efficient quantum computation with linear optics. *Nature* **409**, 46–52 (2001).
27. Raussendorf, R., Browne, D. E. & Briegel, H. J. Measurement-based quantum computation on cluster states. *Phys. Rev. A* **68**, 022312 (2003).
28. Duan, L.-M. & Kimble, H. Scalable photonic quantum computation through cavity-assisted interactions. *Phys. Rev. Lett.* **92**, 127902 (2004).
29. Kimble, H. J. The quantum internet. *Nature* **453**, 1023–1030 (2008).
30. Varnava, M., Browne, D. E. & Rudolph, T. Loss tolerance in one-way quantum computation via counterfactual error correction. *Phys. Rev. Lett.* **97**, 120501 (2006).
31. Pastawski, F., Yoshida, B., Harlow, D. & Preskill, J. Holographic quantum error-correcting codes: toy models for the bulk/boundary correspondence. *J. High Energy Phys.* **2015**, 149 (2015).
32. Grankin, A., Guimond, P., Vasilyev, D., Vermersch, B. & Zoller, P. Free-space photonic quantum link and chiral quantum optics. *Phys. Rev. A* **98**, 043825 (2018).
33. Saffman, M. & Walker, T. Creating single-atom and single-photon sources from entangled atomic ensembles. *Phys. Rev. A* **66**, 065403 (2002).
34. Schön, C., Solano, E., Verstraete, F., Cirac, J. I. & Wolf, M. M. Sequential generation of entangled multiqubit states. *Phys. Rev. Lett.* **95**, 110503 (2005).
35. Lindner, N. H. & Rudolph, T. Proposal for pulsed on-demand sources of photonic cluster state strings. *Phys. Rev. Lett.* **103**, 113602 (2009).
36. Schwartz, I. et al. Deterministic generation of a cluster state of entangled photons. *Science* **354**, 434–437 (2016).
37. Raussendorf, R., Harrington, J. & Goyal, K. Topological fault-tolerance in cluster state quantum computation. *New J. Phys.* **9**, 199 (2007).
38. Jaksch, D. et al. Fast quantum gates for neutral atoms. *Phys. Rev. Lett.* **85**, 2208 (2000).
39. Economou, S. E., Lindner, N. & Rudolph, T. Optically generated 2-dimensional photonic cluster state from coupled quantum dots. *Phys. Rev. Lett.* **105**, 093601 (2010).
40. Barredo, D., De Léséleuc, S., Lienhard, V., Lahaye, T. & Browaeys, A. An atom-by-atom assembler of defect-free arbitrary two-dimensional atomic arrays. *Science* **354**, 1021–1023 (2016).
41. Endres, M. et al. Atom-by-atom assembly of defect-free one-dimensional cold atom arrays. *Science* **354**, 1024–1027 (2016).
42. Kim, H. et al. In situ single-atom array synthesis using dynamic holographic optical tweezers. *Nat. Commun.* **7**, 13317 (2016).
43. Bernien, H. et al. Probing many-body dynamics on a 51-atom quantum simulator. *Nature* **551**, 579–584 (2017).
44. Lienhard, V. et al. Observing the space-and time-dependent growth of correlations in dynamically tuned synthetic Ising models with antiferromagnetic interactions. *Phys. Rev. X* **8**, 021070 (2018).
45. Omran, A. et al. Generation and manipulation of Schrödinger cat states in Rydberg atom arrays. *Science* **365**, 570–574 (2019).
46. Covey, J. P. et al. Telecom-band quantum optics with ytterbium atoms and silicon nanophotonics. *Phys. Rev. Appl.* **11**, 034044 (2019).
47. Rui, J. et al. A subradiant optical mirror formed by a single structured atomic layer. Preprint at https://arxiv.org/pdf/2001.00795.pdf (2020).
48. Li, L., Dudin, Y. & Kuzmich, A. Entanglement between light and an optical atomic excitation. *Nature* **498**, 466–469 (2013).
49. Cooper, A. et al. Alkaline-earth atoms in optical tweezers. *Phys. Rev. X* **8**, 041055 (2018).
50. Bloch, I. Ultracold quantum gases in optical lattices. *Nat. Phys.* **1**, 23–30 (2005).
51. Yu, N. et al. A broadband, background-free quarter-wave plate based on plasmonic metasurfaces. *Nano Lett.* **12**, 6328–6333 (2012).
52. Estakhri, N. M., Edwards, B. & Engheta, N. Inverse-designed metastructures that solve equations. *Science* **363**, 1333–1338 (2019).
53. Lang, J., Chang, D. E. & Piazza, F. Interaction-induced transparency for strong-coupling polaritons. Preprint at https://arxiv.org/pdf/1810.12912.pdf (2018).
54. J. Lang, J., Chang, D. E. & Piazza, F. Non-equilibrium diagrammatic approach to strongly interacting photons. Preprint at https://arxiv.org/pdf/1810.12921.pdf (2018).
55. Zhou, Y. et al. Probing dark excitons in atomically thin semiconductors via near-field coupling to surface plasmon polaritons. *Nat. Nanotechnol.* **12**, 856–860 (2017).
56. Scuri, G. et al. Large excitonic reflectivity of monolayer MoSe$_2$ encapsulated in hexagonal boron nitride. *Phys. Rev. Lett.* **120**, 037402 (2018).

Data availability
The data that support the findings of this study are available from the corresponding author upon reasonable request.

Author contributions
The theoretical analysis and numerical analysis were carried out by R.B. All authors contributed to the development of theoretical tools, discussed the results and contributed to the manuscript. The manuscript was written by R.B., H.P. and M.D.L.

Competing interests
The authors declare no competing interests.

Additional information
Supplementary information is available for this paper at https://doi.org/10.1038/s41567-020-0845-5.

Correspondence and requests for materials should be addressed to R.B.

Reprints and permissions information is available at www.nature.com/reprints.